AGU PUBLICATIONS

Geophysical Research Letters

RESEARCH LETTER
10.1002/2015GL065802

Key Points:
- Low in situ Vp/Vs ratio dominating the summit caldera
- High in situ Vp/Vs ratios observed east and north of Halema'uma'u crater
- The anomalous features can be explained by theoretical modeling and consistent with other data

Supporting Information:
- Figure S1 caption
- Figure S1

Correspondence to:
G. Lin,
glin@rsmas.miami.edu

Citation:
Lin, G., F. Amelung, P. M. Shearer, and P. G. Okubo (2015), Location and size of the shallow magma reservoir beneath Kīlauea caldera, constraints from near-source V_p/V_s ratios, *Geophys. Res. Lett.*, *42*, 8349–8357, doi:10.1002/2015GL065802.

Received 14 AUG 2015
Accepted 2 OCT 2015
Accepted article online 5 OCT 2015
Published online 24 OCT 2015

Location and size of the shallow magma reservoir beneath Kīlauea caldera, constraints from near-source V_p/V_s ratios

Guoqing Lin[1], Falk Amelung[1], Peter M. Shearer[2], and Paul G. Okubo[3]

[1]Department of Marine Geosciences, Rosenstiel School of Marine and Atmospheric Science, University of Miami, Coral Gables, Florida, USA, [2]Institute of Geophysics and Planetary Physics, Scripps Institution of Oceanography, University of California, San Diego, La Jolla, California, USA, [3]Hawaiian Volcano Observatory, U.S. Geological Survey, Hawai'i Volcanoes National Park, Hawaii, USA

Abstract We present high-resolution compressional wave to shear wave velocity ratios (V_p/V_s) beneath Kīlauea's summit caldera by applying an in situ estimation method using waveform cross-correlation data for three similar earthquake clusters. We observe high V_p/V_s ratios (1.832 and 1.852) for two event clusters surrounded by the low background V_p/V_s value of 1.412 at ~2.1 km depth below the surface. These high and low V_p/V_s ratios can be explained by melt- and CO_2-filled cracks, respectively, based on a theoretical crack model. The event cluster with the highest V_p/V_s ratio consists of long-period events that followed the 1997 East Rift Zone eruption, indicating their association with fluid and magma movement. The depths of the two clusters with high V_p/V_s ratios are consistent with the magma reservoir location inferred from geodetic observations. Their locations east and north of Halema'uma'u crater suggest a horizontal extent of a few kilometers for the reservoir.

1. Introduction

The evolution of Kīlauea volcano in Hawai'i and other basaltic shield volcanos is characterized by cyclic collapse and subsequent filling of the summit caldera [*Holcomb et al.*, 1988; *Howard*, 2010]. At Kīlauea, the last caldera collapse occurred about 500 years ago, when the summit collapsed into a previously evacuated magma reservoir, possibly during a cycle of low magma supply rate [*Swanson et al.*, 2014]. Caldera collapse requires an underlying magma reservoir of comparable horizontal extent [e.g., *Acocella*, 2007]. However, at Kīlauea, geodetic and petrologic observations have revealed a reservoir system consisting of multiple, interconnected magma bodies within and south of the caldera [*Baker and Amelung*, 2012; *Poland et al.*, 2014; *Pietruszka et al.*, 2015], rather than a single caldera-wide reservoir. The principal magma body next to Halema'uma'u crater, which feeds the summit eruption, is very small with inferred volume of ~1 km^3 [*Anderson et al.*, 2015; *Pietruszka et al.*, 2015]. The lack of a caldera-wide magma reservoir at Kīlauea is contrasting to other basaltic shield volcanos, such as in the Galapagos Islands and in Iceland, which have central reservoirs with horizontal extent approximate to the caldera diameter [*Amelung et al.*, 2000; *Chadwick et al.*, 2011; *Bagnardi and Amelung*, 2012; *Poland et al.*, 2014].

Geodesy and petrology are capable of observing magma storage zones that experience pressure changes and/or feed eruptions, respectively. Three-dimensional (3-D) seismic tomography has the potential to identify magma storage zones that do not cause ground inflation. The low compressional wave velocity (V_p) zones beneath Kīlauea's summit have been interpreted as the seismic expression of a summit magma reservoir [e.g., *Thurber*, 1984, 1987; *Rowan and Clayton*, 1993; *Dawson et al.*, 1999; *Park et al.*, 2007, 2009]. However, it is difficult to resolve the exact location and size of the magma storage zones because of the limited spatial resolution.

In this study, we estimate the in situ V_p/V_s ratios in the near-source regions beneath Kīlauea's summit caldera by applying a high-resolution estimation method for similar event clusters. The in situ method is able to resolve small-scale, near-source velocity structures to constrain the magma and fluid content under the caldera.

2. In Situ V_p/V_s Ratio Estimates

The V_p/V_s ratio estimate method that we apply in this study was developed and presented by *Lin and Shearer* [2007]. They show that when both *P* and *S* wave differential times from waveform cross correlation are

Table 1. Characteristics of the Three Earthquake Clusters in This Study[a]

Cluster	No. of Events	In Situ V_p/V_s	Uncertainty	Depth (km bsl)	Average Distance (km)	Maximum Distance (km)
1	1312	1.412	0.000	1.09	0.58	5.64
2	53	1.832	0.012	1.20	0.19	2.41
3	92	1.852	0.026	1.06	0.37	1.75

[a]Note that the distances in the last two columns are the interevent distance within each cluster and the uncertainty of the in situ V_p/V_s ratio for cluster 1 is close to zero.

available for similar earthquake clusters, it is possible to estimate near-source V_p/V_s ratios with higher precisions than typical tomographic inversion methods, owing to the great accuracy of the waveform cross-correlation data and a robust misfit function method.

The work in this study is based on the newly developed 3-D seismic velocity model, earthquake relocation catalog, and differential times from waveform cross correlation by *Lin et al.* [2014]. We apply the in situ V_p/V_s estimate approach to the 337 similar event clusters consisting of 25,820 earthquakes on the entire island of Hawai'i from *Lin et al.* [2014] and estimate standard uncertainties in the in situ V_p/V_s ratios. These uncertainties are computed using a bootstrap approach [e.g., *Efron and Gong*, 1983; *Efron and Tibshirani*, 1991], in which the pairs of differential *P* and *S* times in the same cluster are randomly resampled 1000 times. As suggested by *Lin and Shearer* [2007], the most accurate V_p/V_s results for real data clusters are obtained for clusters with three-dimensional distributions of events. In order to estimate the spatial distribution of events in each cluster, we used the method of principal component analysis [e.g., *Kirschvink*, 1980] to compute eigenvalues for the covariance matrix of the earthquake locations for all similar event clusters. Clusters are considered to have nearly spherical distribution if $\lambda_1/\lambda_3 \leq K$, (where eigenvalues $\lambda_1 \geq \lambda_2 \geq \lambda_3$ and K is a constant). This approach has been applied in previous earthquake studies [e.g., *Michelini and Bolt*, 1986; *Shearer et al.*, 2003; *Lin and Thurber*, 2012; *Lin*, 2013].

3. Results

In this study, we select the clusters with $\lambda_1/\lambda_3 \leq 5$ and the estimated standard errors in V_p/V_s less than 0.03 beneath Kīlauea's summit caldera for further analyses. The resulting three clusters (referred as cluster 1–3) consist of 1457 well-relocated events and over 0.22 million differential times. The maximum interevent distance is 5.64, 2.41, and 1.75 km for the three clusters, respectively, and the average distance is below 0.58 km for all the clusters. The estimated in situ V_p/V_s ratios are 1.412 ± 0.000, 1.832 ± 0.012, and 1.852 ± 0.026 for the three selected clusters. The uncertainty for the largest cluster is zero owing to the great number of earthquakes and differential times in the cluster used in the computation. The characteristics of the three earthquake clusters are summarized in Table 1.

In Figures 1a–1c, we show map views of the 3-D V_p model from *Lin et al.* [2014] for Kīlauea's summit area. Zero depth corresponds to mean sea level (~1 km below ground surface). At 1 km depth below sea level (bsl), the caldera area is characterized by lower V_p values than the nearby Upper East Rift Zone and the Southwest Rift Zone. A low-velocity body with up to −9% perturbations relative to the layer average value (5.67 km/s) is observed at 3 km depth bsl (enclosed by the black box in Figure 1b) but not at 6 km depth bsl (Figure 1c).

Map views of the 3-D tomographic V_p/V_s model at 1 and 3 km depths bsl are shown in Figures 1d and 1e. Relatively low to normal V_p/V_s ratios (1.66 to 1.74) are observed at 3 km depth corresponding to the low V_p body. Another noticeable feature is the V_p/V_s anomaly beneath Kīlauea Iki crater. The low V_p/V_s and slightly higher than the layer average V_p anomalies at 1 km depth can be explained by a combination of different mafic compositions, whereas the high V_p/V_s and high V_p anomalies at 3 km depth can be interpreted as mafic magmatic cumulates. The centers of the three similar earthquake clusters are shown as pink stars in Figure 1e. Epicenters of the events in these clusters are plotted in Figure 1f colored by their in situ V_p/V_s ratios. Note that events in each cluster have the same V_p/V_s ratios, therefore the same colors. The caldera area is dominated by low V_p/V_s ratio of 1.412 distributed in the largest cluster (cluster 1) with the center located at 1.09 km depth. To test the robustness of this result and whether it truly applies across the cluster, we split cluster 1 into subclusters and estimate the in situ V_p/V_s ratios. These ratios are all very low and close to the average value for the entire cluster. We also examined event pairs with different correlation coefficients and found that they all maintain the low V_p/V_s ratio. Therefore, we believe that the low V_p/V_s ratio for cluster 1 is a reliable result

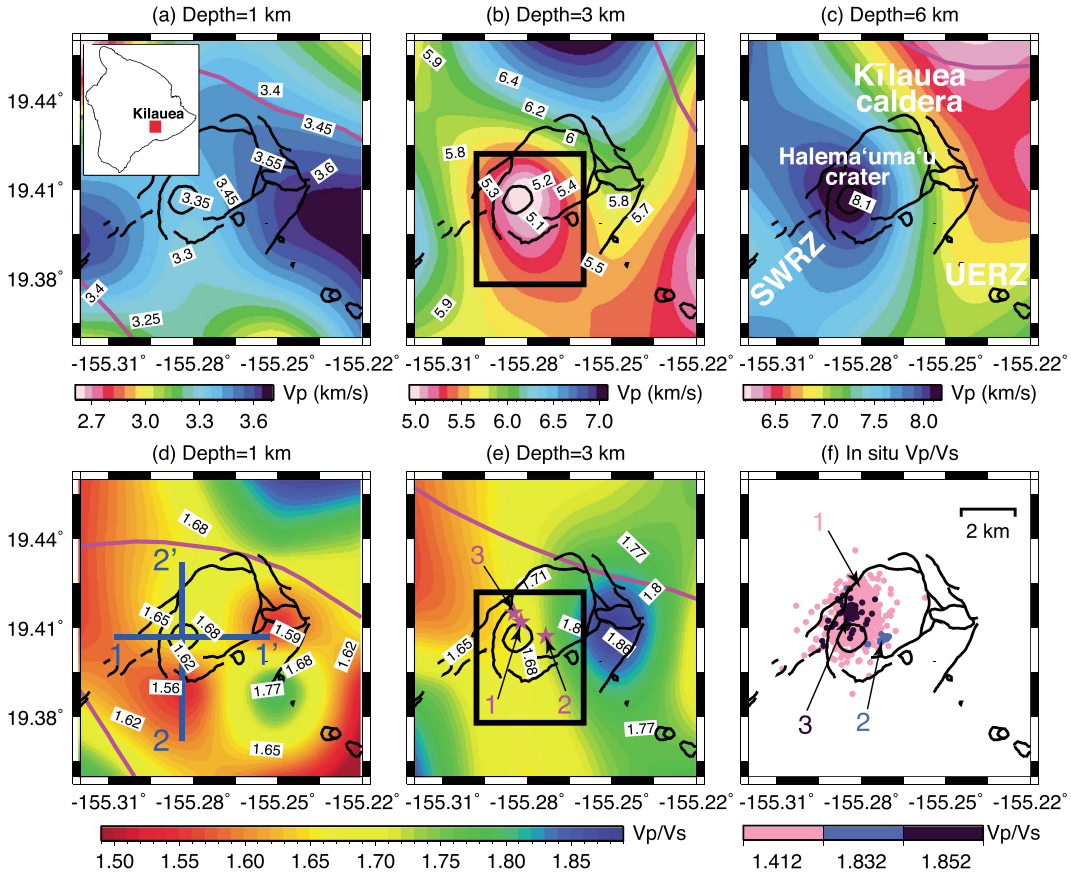

Figure 1. Map views of the (a–c) tomographic *P* wave velocity model and (d and e) V_p/V_s ratios at different depth slices. Pink contours enclose the well-resolved area with the diagonal element of the resolution matrix greater than 0.5. Small red square in the inset map of Figure 1a shows the location of our study area on the island of Hawai'i. Black box in Figures 1b and 1e confines the location of the low V_p body. Major geological structures are marked in Figure 1c, including Kīlauea caldera, Halema'uma'u crater, the Southwest Rift Zone (SWRZ), and the Upper East Rift Zone (UERZ). Blue straight lines in Figure 1d are the profiles for the cross-sectional views shown in Figure 2. Pink stars in Figure 1e represent the centers of the three similar earthquake clusters for the in situ V_p/V_s estimates. (f) Events within similar event clusters, colored by in situ V_p/V_s ratio for each cluster.

owing to the great numbers of events and differential times used in the calculation. Relatively high V_p/V_s values of 1.832 and 1.852 are seen in the surrounding area of Halema'uma'u crater, concentrated on its east (cluster 2) and north (cluster 3) sides, at 1.20 and 1.06 km depths, respectively.

In Figure 2, we show cross sections of the tomographic V_p, V_p/V_s models by *Lin et al.* [2014] and in situ V_p/V_s ratios from the surface (~1 km above sea level) to 6 km depth bsl along two profiles passing through Halema'uma'u crater. The low V_p body between 0.8 and 4.2 km depth bsl beneath the summit caldera is clearly seen in both sections (black boxes in Figures 2a and 2b). The high V_p/V_s ratios from the in situ estimate method are located right on top of this anomalous body. However, the tomographic V_p/V_s model (Figures 2c and 2d) corresponding to this body is dominated by relatively low anomalies (1.62–1.72), instead of high values that are usually expected for magma reservoirs. As seen in the map views, the caldera is dominated by low in situ V_p/V_s ratios, but relatively high values of 1.832 and 1.852 for two similar event clusters are observed centered at ~1.1 km depth bsl, although their horizontal locations are ~1.56 km apart.

4. Discussion

4.1. Earthquake Location Uncertainties

The simul2000 algorithm [*Thurber*, 1983, 1993; *Evans et al.*, 1994; *Thurber and Eberhart-Phillips*, 1999], which was used to develop the 3-D tomographic velocity model by *Lin et al.* [2014], provides the hypocenter error ellipse for each single event. The absolute location uncertainties are computed as the largest of the horizontal

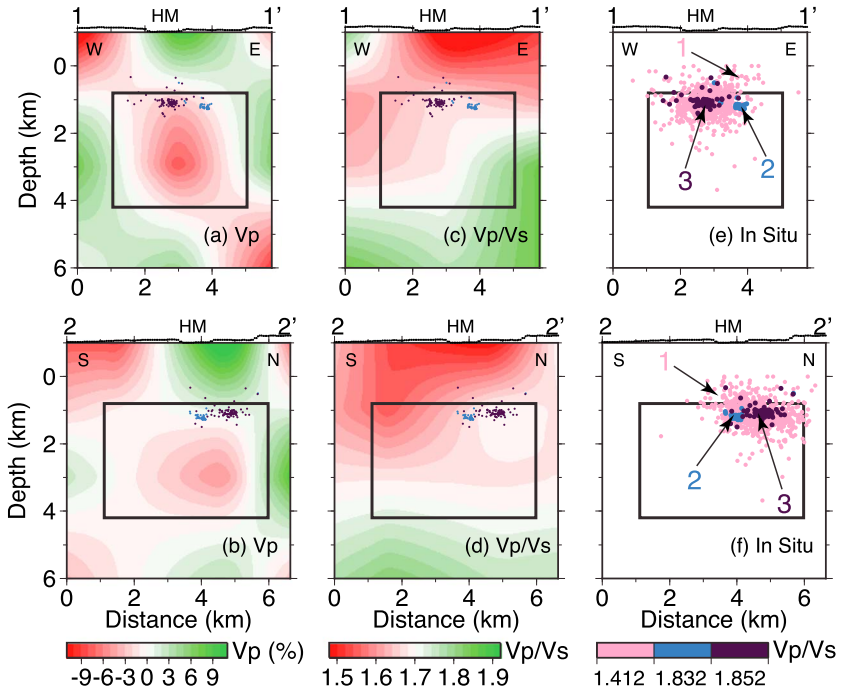

Figure 2. Cross sections of the 3-D tomographic V_p, V_p/V_s models and seismicity distribution along two profiles shown in Figure 1d. Dots represent the waveform cross-correlation relocated earthquakes from *Lin et al.* [2014] within ±5 km of the profile. Zero depth corresponds to mean sea level. The black boxes enclose the low V_p body. HM is the abbreviation for Halema'uma'u crater. Dotted curves at the top illustrate the local topography. (a, b) Tomographic V_p model relative to the depth average at 0.5 km interval. (c, d) Absolute tomographic V_p/V_s ratios. Both the V_p and V_p/V_s models are well resolved along the two profiles according to our criterion, i.e., the diagonal element of resolution matrix is greater than 0.5. (e, f) Events in similar event clusters colored by in situ V_p/V_s ratios. Clusters with high in situ V_p/V_s ratios are also plotted in the tomographic cross sections of Figures 2a–2d, which are mainly distributed between 0.8 and 1.2 km depth.

and vertical projections of the principal standard errors. For the 1457 events in the three similar event clusters, the median absolute location uncertainty is 58 m in horizontal and 30 m in vertical. The high accuracies in absolute earthquake locations are attributed to the good quality of the seismic data used in the tomographic inversion and excellent resolution of the 3-D velocity model in this area. The relative earthquake location uncertainties are estimated by applying a bootstrap approach [*Efron and Gong*, 1983; *Efron and Tibshirani*, 1991], in which the differential times for each event are randomly resampled. The median relative location uncertainty is 91 m for the horizontal and 51 m for the vertical. For all the three clusters, the vertical uncertainties are smaller than the horizontal ones in both absolute and relative location uncertainties, indicating the well-constrained vertical locations in the summit area.

4.2. Theoretical Crack Models

In order to examine the possible causes for the observed in situ V_p/V_s ratios, we investigated the theoretical crack models discussed in *Shearer* [1988], including the models by *Walsh* [1969], *Kuster and Toksöz* [1974], *O'*Connell and Budiansky [1974], *Garbin and Knopoff* [1975], *Watt et al.* [1976], *O'Connell and Budiansky* [1977], *Berryman* [1980], and *Hudson* [1980, 1981]. The models yield similar results at low crack densities and porosities. In principle, the self-consistent models should provide superior results at high porosities, but we found that in practice the self-consistent model of *O'Connell and Budiansky* [1974] predicted very similar V_p/V_s ratios as the *Kuster and Toksöz* [1974] model for spherical inclusions. However, we prefer to use the Kuster and Toksoz model because it can handle the penny-shaped (ellipsoidal) cracks required to explain our observed very low V_p/V_ss ratio. We use V_p of 6.0 km/s and V_p/V_s ratio of 1.74 as the background values for the host rock and assume ellipsoidal cracks with aspect ratios ranging from 0.001 to 0.3.

The dominating in situ V_p/V_s ratio of 1.412 in cluster 1 is greatly lower than the normal V_p/V_s (~1.74) from the tomographic model. *Gregory* [1976] showed that V_p/V_s varies from 1.42 to 1.98 in most water-saturated rocks and can be dropped to 1.30 to 1.69 for gas-filled pore spaces. The most common factors that can reduce V_p/V_s ratios in magmatic systems are the presence of CO_2 gas and water. Therefore, we assume both CO_2- and

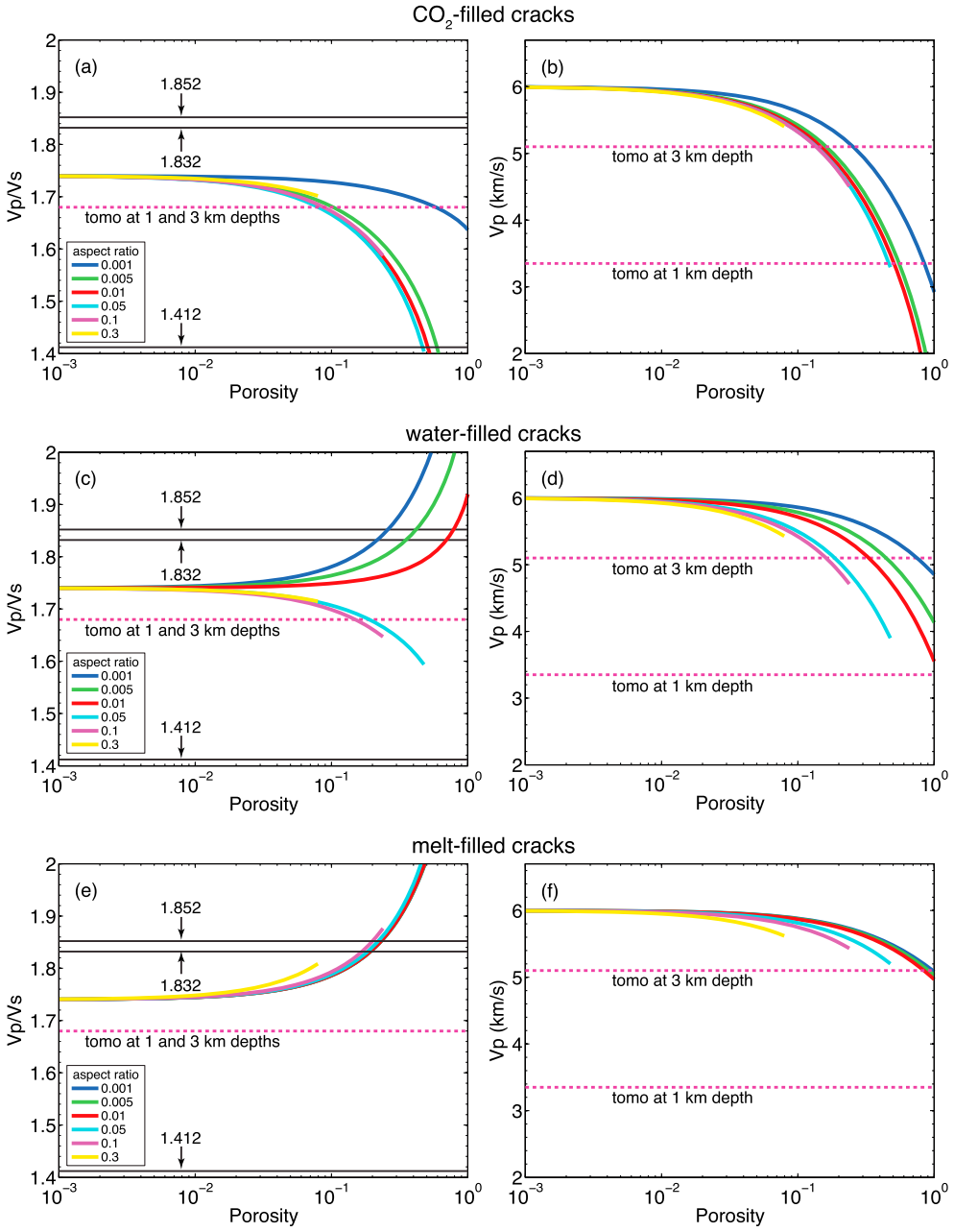

Figure 3. Velocity variations with (a, b) CO_2, (c, d) water, and (e, f) melt inclusions. V_p/V_s ratios (Figures 3a, 3c, and 3e) and V_p values (Figures 3b, 3d, and 3f) as a function of porosity for different aspect ratios according to the theoretical crack model by *Kuster and Toksöz* [1974]. Black horizontal lines in Figures 3a, 3c, and 3e show the in situ V_p/V_s ratios for the three earthquake clusters. Pink dotted ones show the tomographic V_p/V_s (Figures 3a, 3c, and 3e) and V_p (Figures 3b, 3d, and 3f) values for the area where the three clusters are located.

water-filled cracks to compute the possible V_p/V_s ratios. We require V_p of 0.4 km/s and 1.45 km/s and density of 0.75 g/cm^3 and 1.0 g/cm^3 for CO_2- and water-filled cracks, respectively. In Figures 3a and 3b, we show V_p/V_s ratio and V_p value as a function of porosity for CO_2-filled cracks with different aspect ratios according to the theoretical crack model. The V_p/V_s ratio can be reduced to the required value (i.e., 1.412) with porosity of 47–60% and crack aspect ratio of 0.005–0.05. For water-filled cracks (shown in Figures 3c and 3d), the lowest V_p/V_s ratio is ~1.594 with aspect ratio of 0.05 thus is not able to explain the observed low V_p/V_s ratio alone. However, we cannot rule out the possibility of a CO_2-water mixed crack model.

The high in situ V_p/V_s ratios of 1.832 and 1.852 centered at ~1.1 km depth must be explained by another mechanism. High V_p/V_s ratio together with the corresponding low V_p value in active volcanos is often interpreted

as the presence of melt. We apply the same theoretical crack model by *Kuster and Toksöz* [1974] assuming melt-filled cracks in order to determine the porosity and crack aspect ratio that are necessary to increase the V_p/V_s ratio to the observed values. We use the same background velocity and density information for the host rock and assume that the cracks are ellipsoidal and melt filled ($V_p = 3.3$ km/s and $\rho = 2.6$ g/cm^3). In Figures 3e and 3f, we show V_p/V_s and V_p values for melt-filled cracks as a function of porosity for different aspect ratios. The V_p/V_s ratio can be increased to 1.832–1.852 with porosity of 17–24% and aspect ratio of 0.01–0.1, while the corresponding V_p values are reduced from the background value to the average V_p value at 3 km depth from the tomographic model. However, as shown in Figures 3c and 3d, water-filled cracks with small aspect ratios ($\leq$0.01) can also increase V_p/V_s and decrease V_p values. Therefore, it is also likely to have flat water inclusions.

We also examined the robustness of our porosity estimates with respect to the background V_p and V_p/V_s values. Figure S1 in the supporting information shows the required porosities to obtain the target in situ V_p/V_s ratios (i.e., 1.412, 1.832, and 1.852) as a function of the background V_p and V_p/V_s values for an aspect ratio of 0.01. Figure S1a shows that for the background V_p of 5.0–6.5 km/s and V_p/V_s of 1.63–1.83, the required porosity to obtain the target in situ V_p/V_s of 1.412 varies between 49% and 56% and does not show significant dependence on the background V_p/V_s value. Figures S1b and S1c show that the required porosity to obtain the target in situ V_p/V_s of 1.832 and 1.852 varies between 21% and 25% for a typical background V_p/V_s of 1.73 and does not show significant dependence on the background V_p value. Thus, we conclude that different background values will result in slightly different porosities required by the target V_p/V_s but do not change our main conclusions.

Our purpose in this section is to show that our V_p/V_s observations can be roughly explained using the *Kuster and Toksöz* [1974] model, but it should be acknowledged that the high porosities and crack densities that are required challenge the accuracy of the model. Additional tests using more sophisticated composite media theories are therefore warranted.

4.3. Event Type and Time

Long-period (LP) events are often hypothesized to be related with fluid or magma movement. In this section, we look into the event type for events in each cluster and their time span. Cluster 1 with the lowest in situ V_p/V_s ratio of 1.412 covers 14 years of our study period between 1992 and 2009 with 1152 out of 1312 events between 30 January and 16 February 1997. These events may be related with the 1997 East Rift Zone (ERZ) eruption, which lacked precursory summit inflation, probably because of its occurrence in response to a decrease of the rift zone-perpendicular normal stress due to flank motion [*Owen et al.*, 2000; *Segall et al.*, 2001; *Almendros et al.*, 2001; *Desmarais and Segall*, 2007]. The eruption started in the morning of 30 January 1997 and lasted 22 h. We compared these earthquakes with the LP events in *Matoza et al.* [2014] and found out that 451 of them are identified as LP events. *Matoza et al.* [2014] stated that the LP event catalog especially the shallow events can be slightly incomplete. Given the waveform similarity for the events within each cluster, it is plausible to assume that other events in the cluster are also LP events. The time and type of these events suggest that they are related with fluid or magma movement, which may be associated with the magmatic activity after the 1997 ERZ eruption.

Cluster 2 with the in situ V_p/V_s ratio of 1.832 spans 12 years of the entire 17 year time period in this study and consists of no events in 1997 at all. Two out of the 53 events in the cluster are identified as the LP events by *Matoza et al.* [2014]. In cluster 3 with the highest V_p/V_s ratio of 1.852, the 92 events, 64 of which are flagged as the LP events by *Matoza et al.* [2014], only cover 2 weeks between 1 and 15 February 1997, right after the ERZ eruption. The identification of the LP events again supports the postulation of the involvement of fluid and magma. However, the time difference between these two clusters suggests different connections of these events with the corresponding fluid transportation. The longer duration of cluster 2 indicates the lasting reaction to a long-standing activity. The temporary time span of cluster 3 shows more active response to the transient ERZ eruption.

4.4. Comparison With Tomographic Results

Similar to the results for Southern California by *Lin and Shearer* [2009], the high-resolution V_p/V_s ratio estimates for similar event clusters show that there may be fine-scale velocity structure that cannot be easily resolved by tomographic methods. Despite the different absolute values, however, the pattern of the in situ V_p/V_s ratios is consistent with the tomographic model by *Lin et al.* [2014]. In the map view of the tomographic V_p/V_s model at 1 km depth bsl (Figure 1d), the area where cluster 3 is located shows relatively high values of

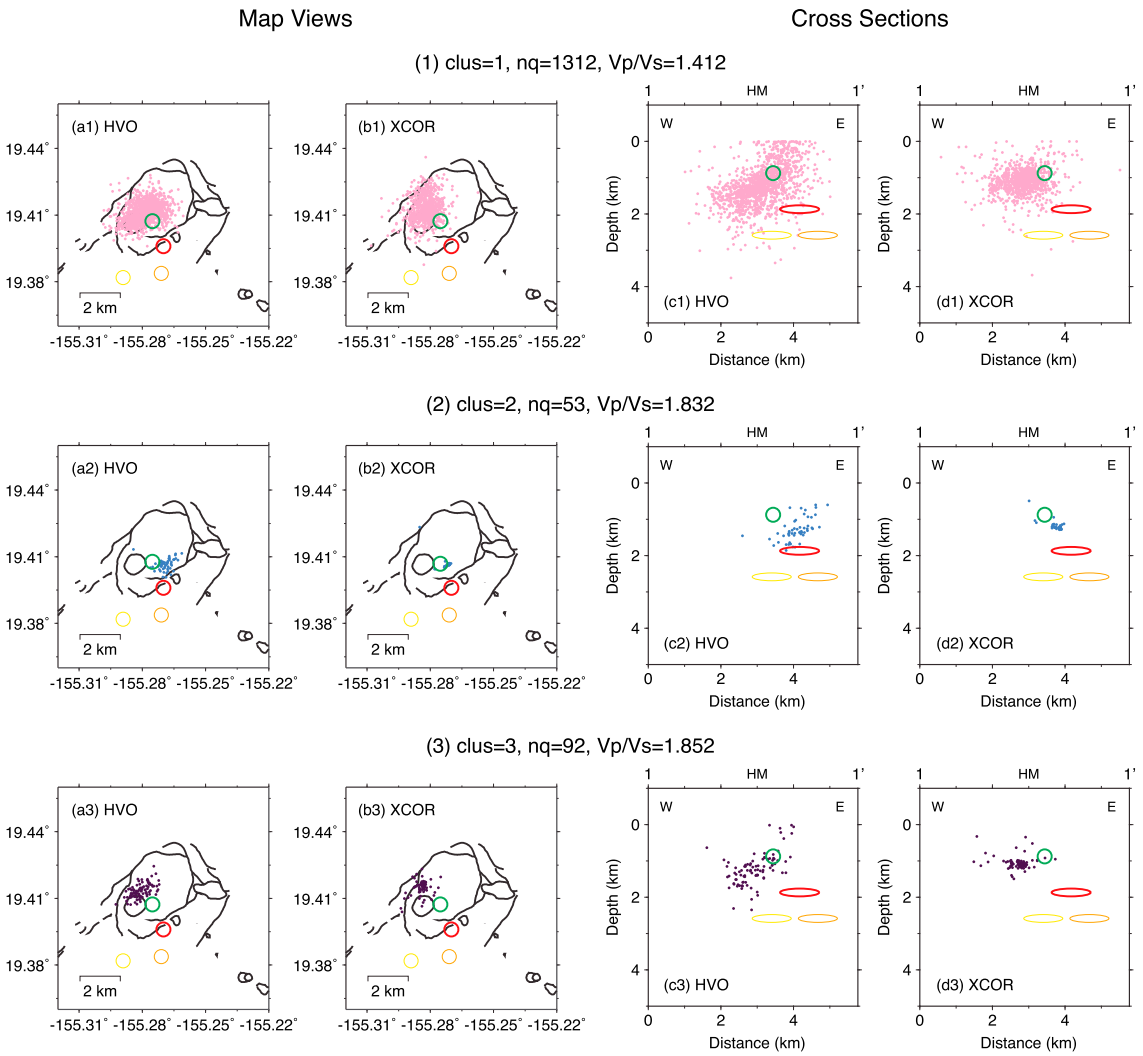

Figure 4. The HVO catalog location and the waveform cross-correlation relocation comparison for the three event clusters of interest in this study. Seismicity within ±5 km of the profile is shown in the cross sections (c1–c3 and d1–d3). Circles and ellipses are the modeled sources of deformation (not to scale) by *Baker and Amelung* [2012] based on geodetic data.

1.68 compared to the surrounding regions, which is between the low and high in situ V_p/V_s ratios. This may indicate that the tomographic model images the average V_p/V_s value in the area. *Lin et al.* [2015] also conclude that the high *P* wave attenuation structure together with the low V_p values above 4 km depth beneath the summit caldera may suggest the presence of magma chamber surrounded by water and/or gas.

4.5. Comparison With Geodetic Sources

Geodetic observations over the past 50 years have identified the summit magma bodies that experienced pressure changes. Kīlauea's main magma body, located just east of Halema'uma'u, inflates and deflates over periods lasting several weeks to months [*Baker and Amelung*, 2012; *Poland et al.*, 2012; *Lundgren et al.*, 2013; *Poland et al.*, 2014; *Baker and Amelung*, 2015] and is the source of the frequent hours-to-days lasting deflation-inflation events [*Anderson et al.*, 2015]. A second, less frequently activated reservoir system consisting of at least three sources is located south of the caldera rim. The reservoir depths are 1.9 km for the Halema'uma'u source and 2.9–3.6 km for the southern caldera sources [*Baker and Amelung*, 2012]. Results from geochemical analysis of lavas from the last 50 years are consistent with this two-tier magma plumbing model [*Pietruszka et al.*, 2015].

Figure 4 shows the earthquake location comparison between the HVO catalog and the waveform cross-correlation locations for the three event clusters of interest, together with the geodetic sources of *Baker and Amelung* [2012]. The events in cluster 2 with high V_p/V_s ratio are located near the Halema'uma'u source

(green circle) in the same depth range, consistent with our interpretation of melt-filled cracks. However, the events in cluster 3 with the highest V_p/V_s ratio are located ~1.3 km to the northwest of this source. The discrepancy between this cluster and the geodetic source location cannot be caused by earthquake mislocations, given our location uncertainty estimates. We infer from the high V_p/V_s ratio of this cluster that magma is present in this part of the caldera.

4.6. Implications

The in situ V_p/V_s ratios are calculated within the source regions of the three similar earthquake clusters. The source region of cluster 1, which we interpret to contain cracks filled with CO_2 gas are spread out under the western part of the caldera. The events in clusters 2 and 3, which we interpret to represent cracks filled with melt, are located near the Halema'uma'u source and north of Halema'uma'u crater, respectively.

The magma detected north of Halema'uma'u may represent a remnant of a larger reservoir that was present prior to the last caldera collapse. This magma body is either very small so that pressure changes do not result in detectable surface deformation or it is not connected to the active Halema'uma'u reservoir. Halema'uma'u had an active lava lake across the entire crater until 1952, which shows that the reservoir was for this time period larger than its current size. We speculate that the rock mass containing the gas-filled cracks from cluster 1 could represent material from the last collapse. The possible presence of void space inferred from gravity change data [*Bagnardi et al.*, 2014] also suggests a complex structure under the caldera, different than the simple picture of a spherical reservoir embedded in a homogenous rock mass. Most of the seismic events of the three clusters are located between sea level and 2 km bsl. We hypothesize that some of these events occurred along surfaces between block leftovers from the previous caldera collapse.

5. Conclusions

In this study, we apply a high-resolution V_p/V_s ratio estimation method to the near-earthquake source region beneath Kīlauea's summit caldera, Hawai'i. High V_p/V_s ratios of 1.832 and 1.852 interpreted as melt are observed to be surrounded by low ratio of 1.412 (presumably CO_2 gas) at ~1.1 km depth bsl (i.e., 2.1 km below the surface). The location and depth of one of the high V_p/V_s clusters agree with the geodetic Halema'uma'u source. The other one located north of Halema'uma'u crater suggests that the summit magma reservoir is much larger than the currently active one, consistent with the presence of a caldera several kilometers across.

Acknowledgments

Seismic data used in this study were obtained and originate from the USGS Hawaiian Volcano Observatory. Previous velocity model, location catalog, and waveform data were collected from published studies listed in the references. We thank the USGS Hawaiian Volcano Observatory for maintaining the seismic network and making the data available. We are grateful to Phil Dawson and two anonymous reviewers for their constructive and detailed comments. Plots were made using the public domain GMT software [*Wessel and Smith*, 1991] and MATLAB. Funding for this research was provided by the National Science Foundation grant EAR-1246935.

References

Acocella, V. (2007), Understanding caldera structure and development: An overview of analogue models compared to natural calderas, *Earth Sci. Rev.*, *85*(3–4), 125–160, doi:10.1016/j.earscirev.2007.08.004.

Almendros, J., B. Chouet, and P. Dawson (2001), Spatial extent of a hydrothermal system at Kilauea Volcano, Hawaii, determined from array analyses of shallow long-period seismicity: 2. Results, *J. Geophys. Res.*, *106*(B7), 13,581–13,597.

Amelung, F., S. Jonsson, H. Zebker, and P. Segall (2000), Widespread uplift and "trapdoor" faulting on Galapagos volcanoes observed with radar interferometry, *Nature*, *407*(6807), 993–996.

Anderson, K. R., M. P. Poland, J. H. Johnson, and A. Miklius (2015), Episodic deflation-inflation events at Kilauea Volcano and implications for the shallow magma system, in *Hawaiian Volcanoes: From Source to Surface, Geophys. Monogr. Ser.*, vol. 208, edited by R. Carey et al., 1st ed., pp. 229–250, John Wiley, Hoboken, N. J.

Bagnardi, M., and F. Amelung (2012), Space-geodetic evidence for multiple magma reservoirs and subvolcanic lateral intrusions at Fernandina Volcano, Galapagos Islands, *J. Geophys. Res.*, *117*, B10406, doi:10.1029/2012JB009465.

Bagnardi, M., M. P. Poland, D. Carbone, S. Baker, M. Battaglia, and F. Amelung (2014), Gravity changes and deformation at Kīlauea Volcano, Hawaii, associated with summit eruptive activity, 2009–2012, *J. Geophys. Res. Solid Earth*, *119*, 7288–7305, doi:10.1002/2014JB011506.

Baker, S., and F. Amelung (2012), Top-down inflation and deflation at the summit of Kilauea Volcano, Hawaii observed with InSAR, *J. Geophys. Res.*, *117*, B12406, doi:10.1029/2011JB009123.

Baker, S., and F. Amelung (2015), Pressurized magma reservoir within the East Rift Zone of Kīlauea Volcano, Hawai'i: Evidence for relaxed stress changes from the 1975 Kalapana earthquake, *Geophys. Res. Lett.*, *42*, 1758–1765, doi:10.1002/2015GL063161.

Berryman, J. G. (1980), Long-wavelength propagation in composite elastic media: II. Ellipsoidal inclusions, *J. Acoust. Soc. Am.*, *68*, 1820–1831, doi:10.1121/1.385172.

Chadwick, W. W., S. Jónsson, D. Geist, M. Poland, D. Johnson, S. Batt, K. Harpp, and A. Ruiz (2011), The May 2005 eruption of Fernandina volcano, Galápagos: The first circumferential dike intrusion observed by GPS and InSAR, *Bull. Volcanol.*, *73*(6), 679–697, doi:10.1007/s00445-010-0433-0.

Dawson, P. B., B. A. Chouet, P. G. Okubo, A. Villaseñor, and H. M. Benz (1999), Three-dimensional velocity structure of the Kilauea Caldera, Hawaii, *Geophys. Res. Lett.*, *26*(18), 2805–2808.

Desmarais, E. K., and P. Segall (2007), Transient deformation following the 30 January 1997 dike intrusion at Kilauea volcano, Hawaii, *Bull. Volcanol.*, *69*(4), 353–363, doi:10.1007/s00445-006-0080-7.

Efron, B., and G. Gong (1983), A leisurely look at the bootstrap, the jackknife and cross-validation, *Am. Stat.*, *37*(1), 36–48.

Efron, B., and R. Tibshirani (1991), Statistical data analysis in the computer age, *Science*, *253*(5018), 390–395.

Evans, J. R., D. Eberhart-Phillips, and C. H. Thurber (1994), User's manual for SIMULPS12 for imaging Vp and Vp/Vs: A derivative of the "Thurber" tomographic inversion SIMUL3 for local earthquakes and explosion, *U.S. Geol. Surv. Open-File Rep. 94-431*, U.S. Geol. Surv., Reston, Va.

Garbin, H. D., and L. Knopoff (1975), Elastic moduli of a medium with liquid filled cracks, *Q. Appl. Math.*, *33*, 301–303.
Gregory, A. (1976), Fluid saturation effects on dynamic elastic properties of sedimentary rocks, *Geophysics*, *41*(5), 895–921, doi:10.1190/1.1440671.
Holcomb, R. T., J. G. Moore, P. W. Lipman, and R. H. Belderson (1988), Voluminous submarine lava flows from Hawaiian volcanoes, *Geology*, *16*(5), 400–404.
Howard, K. A. (2010), Caldera collapse: Perspectives from comparing Galápagos volcanoes, nuclear test sinks, sandbox models, and volcanoes on Mars, *Geol. Soc. Am.*, *20*(10), 4–10, doi:10.1130/GSATG82A.1.
Hudson, J. A. (1980), Overall properties of a cracked solid, *Math. Proc. Cambridge Philos. Soc.*, *88*(92), 371–384, doi:10.1017/S0305004100057674.
Hudson, J. A. (1981), Wave speeds and attenuation of elastic waves in material containing cracks, *Geophys. J. R. Astron. Soc.*, *64*(1), 133–150, doi:10.1111/j.1365-246X.1981.tb02662.x.
Kirschvink, J. L. (1980), The least-squares line and plane and the analysis of palaeomagnetic data, *Geophys. J. R. Astron. Soc.*, *62*(3), 699–718.
Kuster, G. T., and M. N. Toksöz (1974), Velocity and attenuation of seismic waves in two-phase media: Part I. Theoretical formulations, *Geophysics*, *39*(5), 587–606.
Lin, G. (2013), Seismic investigation of magmatic unrest beneath Mammoth Mountain, California using waveform cross-correlation, *Geology*, *41*(8), 847–850, doi:10.1130/G34062.1.
Lin, G., and P. M. Shearer (2007), Estimating local Vp/Vs ratios within similar earthquake clusters, *Bull. Seismol. Soc. Am.*, *97*(2), 379–388.
Lin, G., and P. M. Shearer (2009), Evidence for water-filled cracks in earthquake source regions, *Geophys. Res. Lett.*, *36*, L17315, doi:10.1029/2009GL039098.
Lin, G., and C. H. Thurber (2012), Seismic velocity variations along the rupture zone of the 1989 Loma Prieta earthquake, California, *J. Geophys. Res.*, *117*, B09301, doi:10.1029/2011JB009122.
Lin, G., P. M. Shearer, R. S. Matoza, P. G. Okubo, and F. Amelung (2014), Three-dimensional seismic velocity structure of Mauna Loa and Kilauea volcanoes in Hawaii from local seismic tomography, *J. Geophys. Res. Solid Earth*, *119*, 4377–4392, doi:10.1002/2013JB010820.
Lin, G., P. M. Shearer, F. Amelung, and P. G. Okubo (2015), Seismic tomography of compressional wave attenuation structure for Kīlauea volcano, Hawai'i, *J. Geophys. Res. Solid Earth*, *120*, 2510–2524, doi:10.1002/2014JB011594.
Lundgren, P., et al. (2013), Evolution of dike opening during the March 2011 Kamoamoa fissure eruption, Kilauea Volcano, Hawaii, *J. Geophys. Res. Solid Earth*, *118*, 897–914, doi:10.1002/jgrb.50108.
Matoza, R. S., P. M. Shearer, and P. G. Okubo (2014), High-precision relocation of long-period events beneath the summit region of Kīlauea Volcano, Hawai'i, from 1986 to 2009, *Geophys. Res. Lett.*, *41*, 3413–3421, doi:10.1002/2014GL059819.
Michelini, A., and B. A. Bolt (1986), Application of the principal parameters method to the 1983 Coalinga, California, aftershock sequence, *Bull. Seismol. Soc. Am.*, *76*(2), 409–420.
O'Connell, R. J., and B. Budiansky (1974), Seismic velocities in dry and saturated cracked solids, *J. Geophys. Res.*, *79*(35), 5412–5426.
O'Connell, R. J., and B. Budiansky (1977), Viscoelastic properties of fluid-saturated cracked solids, *J. Geophys. Res.*, *82*(36), 5719–5735.
Owen, S., P. Segall, M. Lisowski, A. Miklius, M. Murray, M. Bevis, and J. Foster (2000), January 30, 1997 eruptive event on Kilauea Volcano, Hawaii, as monitored by continuous GPS, *Geophys. Res. Lett.*, *27*(17), 2757–2760.
Park, J., J. K. Morgan, C. A. Zelt, P. G. Okubo, L. Peters, and N. Benesh (2007), Comparative velocity structure of active Hawaiian volcanoes from 3-D onshore-offshore seismic tomography, *Earth Planet. Sci. Lett.*, *259*(3–4), 500–516, doi:10.1016/j.epsl.2007.05.008.
Park, J., J. K. Morgan, C. A. Zelt, and P. G. Okubo (2009), Volcano-tectonic implications of 3-D velocity structures derived from joint active and passive source tomography of the island of Hawaii, *J. Geophys. Res.*, *114*, B09301, doi:10.1029/2008JB005929.
Pietruszka, A. J., D. E. Heaton, J. P. Marske, and M. O. Garcia (2015), Two magma bodies beneath the summit of Kīlauea Volcano unveiled by isotopically distinct melt deliveries from the mantle, *Earth. Planet. Sc. Lett.*, *413*, 90–100, doi:10.1016/j.epsl.2014.12.040.
Poland, M. P., A. Miklius, A. Jeff Sutton, and C. R. Thornber (2012), A mantle-driven surge in magma supply to Kilauea Volcano during 2003–2007, *Nat. Geosci.*, *5*(4), 295–300.
Poland, M. P., A. Miklius, and E. K. Montgomery-Brown (2014), Magma supply, storage, and transport at shield-stage Hawaiian volcanoes, in *Characteristics of Hawaiian Volcanoes, U.S. Geol. Surv. Prof. Pap. 1801*, edited by M. P. Poland, T. J. Takahashi, and C. M. Landowski, pp. 1–56, U.S. Geol. Surv., Reston, Va.
Rowan, L., and R. W. Clayton (1993), The three-dimensional structure of Kilauea Volcano, Hawaii, from travel time tomography, *J. Geophys. Res.*, *98*(B3), 4355–4375.
Segall, P., P. Cervelli, S. Owen, M. Lisowski, and A. Miklius (2001), Constraints on dike propagation from continuous GPS measurements, *J. Geophys. Res.*, *106*(B9), 19,301–19,317.
Shearer, P. M. (1988), Cracked media, Poisson's ratio, and the structure of the upper oceanic crust, *Geophys. J.*, *92*, 357–362.
Shearer, P. M., J. L. Hardebeck, L. Astiz, and K. B. Richards-Dinger (2003), Analysis of similar event clusters in aftershocks of the 1994 Northridge, California, earthquake, *J. Geophys. Res.*, *108*(B1), 2035, doi:10.1029/2001JB000685.
Swanson, D. A., T. R. Rose, A. E. Mucek, M. O. Garcia, R. S. Fiske, and L. G. Mastin (2014), Cycles of explosive and effusive eruptions at Kīlauea Volcano, Hawai'i, *Geology*, *42*(7), 631–634, doi:10.1130/G35701.1.
Thurber, C. (1984), Seismic detection of the summit magma complex of Kilauea volcano, Hawaii, *Science*, *223*(4632), 165–167.
Thurber, C., and D. Eberhart-Phillips (1999), Local earthquake tomography with flexible gridding, *Comput. Geosci.*, *25*, 809–818.
Thurber, C. H. (1983), Earthquake locations and three-dimensional crustal structure in the Coyote Lake area, central California, *J. Geophys. Res.*, *88*(B10), 8226–8236.
Thurber, C. H. (1987), Seismic structure and tectonics of Kilauea Volcano, *U.S. Geol. Surv. Prof. Pap.*, *1350*, 919–934.
Thurber, C. H. (1993), Local earthquake tomography: Velocities and Vp/Vs-theory, in *Seismic Tomography: Theory and Practice*, edited by H. M. Iyer and K. Hirahara, pp. 563–583, Chapman and Hall, London.
Walsh, J. B. (1969), New analysis of attenuation in partially melted rock, *J. Geophys. Res.*, *74*, 4333–4337.
Watt, J. P., G. F. Davies, and R. J. O'Connell (1976), The elastic properties of composite materials, *Rev. Geophys.*, *14*(4), 541–563.
Wessel, P., and W. H. F. Smith (1991), Free software helps map and display data, *Eos Trans. AGU*, *72*, 441–446.